# Abrupt global-ocean anoxia during the Late Ordovician–early Silurian detected using uranium isotopes of marine carbonates

Rick Bartlett[a,b], Maya Elrick[a,1], James R. Wheeley[c], Victor Polyak[a], André Desrochers[d], and Yemane Asmerom[a]

[a]Earth and Planetary Sciences, University of New Mexico, Albuquerque, NM 87131; [b]Department of Geology and Geophysics, Louisiana State University, Baton Rouge, LA 70803; [c]Geography, Earth and Environmental Sciences, University of Birmingham, Birmingham B15 2TT, United Kingdom; and [d]Earth and Environmental Sciences, University of Ottawa, Ottawa ON K1N 6N5, Canada

Edited by Edward A. Boyle, Massachusetts Institute of Technology, Cambridge, MA, and approved April 10, 2018 (received for review February 21, 2018)

**Widespread marine anoxia is hypothesized as the trigger for the second pulse of the Late Ordovician (Hirnantian) mass extinction based on lithologic and geochemical proxies that record local bottom waters or porewaters. We test the anoxia hypothesis using $\delta^{238}U$ values of marine limestones as a global seawater redox proxy. The $\delta^{238}U$ trends at Anticosti Island, Canada, document an abrupt late Hirnantian ∼0.3‰ negative shift continuing through the early Silurian indicating more reducing seawater conditions. The lack of observed anoxic facies and no covariance among $\delta^{238}U$ values and other local redox proxies suggests that the $\delta^{238}U$ trends represent a global-ocean redox record. The Hirnantian ocean anoxic event (HOAE) onset is coincident with the extinction pulse indicating its importance in triggering it. Anoxia initiated during high sea levels before peak Hirnantian glaciation, and continued into the subsequent lowstand and early Silurian deglacial eustatic rise, implying that major climatic and eustatic changes had little effect on global-ocean redox conditions. The HOAE occurred during a global $\delta^{13}C$ positive excursion, but lasted longer indicating that controls on the C budget were partially decoupled from global-ocean redox trends. U cycle modeling suggests that there was a ∼15% increase in anoxic seafloor area and ∼80% of seawater U was sequestered into anoxic sediments during the HOAE. Unlike other ocean anoxic events (OAE), the HOAE occurred during peak and waning icehouse conditions rather than during greenhouse climates. We interpret that anoxia was driven by global cooling, which reorganized thermohaline circulation, decreased deep-ocean ventilation, enhanced nutrient fluxes, stimulated productivity, which lead to expanded oxygen minimum zones.**

Late Ordovician extinction | U isotopes | seawater redox | ocean anoxic event | glaciation

The Ordovician (∼485–444 My) was a dynamic time interval that recorded a greenhouse-to-icehouse climatic transition, the first Phanerozoic glaciation peaking in the latest Ordovician (Hirnantian stage), and a major increase in biologic diversity punctuated by the first of the "big five" Phanerozoic mass extinctions (Late Ordovician mass extinction [LOME]; refs. 1–3). The LOME resulted in the loss of ∼85% of marine species and occurred in two discrete pulses, one at the beginning of the Hirnantian and the other about 1.0 My later, near the end of the Hirnantian (2, 3). The first pulse is traditionally attributed to cooling, glacio-eustatic sea-level fall and loss of shallow-marine habitats (4, 5); however, this interpretation was recently challenged using detailed sequence stratigraphic and associated biologic diversity data and is now interpreted as occurring during a deglaciation and eustatic sea-level rise (6). Marine anoxia is commonly implicated in the second extinction pulse based on the occurrence of widespread organic-rich marine facies accumulating during and after the extinction pulse and from geochemical redox proxy trends including pyrite sulfur isotopes, redox sensitive trace elements, pyrite framboid-size distributions, and Fe speciation (7, 8–10). The anoxia-driven extinction hypothesis suggests that anoxic/euxinic waters spread onto shallow-shelf habitats and poisoned shallow-marine benthic animals, and that this occurred during the deglaciation after peak Hirnantian glacial conditions (3, 11, 12).

Two lines of evidence call the existing anoxia-driven extinction hypothesis into question. First, geochemical and lithologic redox proxies utilized for the interpretation evaluate local bottom water or porewater conditions, thus do not assess global-ocean redox trends. In addition, the redox trends represent conditions derived from epeiric seaway deposits (versus the open ocean deposits), which represent only a portion of the global ocean seafloor. Second, the previous anoxia-driven interpretations were derived from various geographically separated locations, each providing biologic, geochemical, or sea-level records that require biostratigraphy and/or carbon isotope stratigraphy for correlation among the different locations. These correlations do not provide sufficient temporal resolution to evaluate precise timing relationships among the rapidly changing paleoenvironmental conditions.

To develop a high-resolution, globally integrated seawater redox curve across the second LOME pulse and to alleviate potential timing mismatches among associated rapid climatic, biologic, and geochemical events, we utilize uranium (U) isotopes from Upper Ordovician–lower Silurian marine limestones of Anticosti Island, Canada. It has been shown that $^{238}U/^{235}U$ isotopic ratios in marine carbonates can serve as a proxy for

## Significance

**The Late Ordovician mass extinction (LOME) terminated one of the greatest biodiversity radiations in Earth history eliminating ∼85% of marine animals, and it is coincident with the first major glaciation of the Phanerozoic. To evaluate LOME origins, we use uranium isotopes from marine limestones as a proxy for global-ocean redox conditions. Our results provide evidence of an abrupt global-ocean anoxic event coincident with the LOME onset and its continuation after the biologic recovery, through peak glaciation, and the following early Silurian deglaciation. These results also provide evidence for widespread ocean anoxia initiating and continuing during icehouse conditions.**

Author contributions: M.E. designed research; R.B., M.E., J.R.W., and A.D. performed research; R.B., M.E., J.R.W., V.P., and A.D. analyzed data; and R.B., M.E., J.R.W., V.P., A.D., and Y.A. wrote the paper.

The authors declare no conflict of interest.

This article is a PNAS Direct Submission.



[1]To whom correspondence should be addressed. Email: dolomite@unm.edu.

This article contains supporting information online at www.pnas.org/lookup/suppl/doi:10.1073/pnas.1802438115/-/DCSupplemental.

Published online May 21, 2018.

global-ocean redox conditions and provide a means of quantifying changes in the extent of anoxic sediment accumulation across a range of geologic time intervals (13–18). This is because $^{238}$U(IV) is preferentially sequestered into anoxic marine sediments leaving the residual U(VI) in seawater with a lower $^{238}$U/$^{235}$U ratio, which is subsequently incorporated into carbonate sediments (19, 20). In the modern era, uranium has a long ocean residence time (~400 ky) relative to ocean mixing time (<1 ky), therefore local measurements have the potential to represent global seawater redox conditions.

We focus on the western Anticosti Island section because it is one of the best-studied limestone-dominated Ordovician–Silurian (O–S) boundary sections in the world (*SI Appendix*) and provides a well-dated record of glacio-eustatic, biodiversity, and geochemical trends derived from a single location (Laframboise section; refs. 6, 10, and 21–24). Given that all of the proxy data are derived from the same section, there are no temporal miscorrelations among the different datasets and direct relationships among paleoenvironmeal changes can be evaluated. The specific objectives of this study are to (*i*) describe and interpret U-isotope, elemental, and apatite-based $\delta^{18}$O trends across the Upper Ordovician–lower Silurian, and (*ii*) test the role of ocean anoxia during an icehouse climate as a possible cause for the second LOME pulse—one of the five biggest mass extinctions in Earth history.

## Geologic and U-Isotope Geochemistry Background

Globally high sea levels throughout most of the Ordovician generated vast epeiric seas and resultant abundant shallow-marine environments. Upper Ordovician through lower Silurian limestones on Anticosti Island were deposited in southern subtropical paleolatitudes and are composed of bioturbated offshore through upper shoreface and patch reef facies (ref. 21 and *SI Appendix*, Fig. S1). Two LOME extinction pulses are recorded at Anticosti Island and include benthic, planktic, and nektonic organisms (ref. 6, their figure 3). The previously reported Hirnantian positive carbon isotope excursion (HICE) recorded at western Anticosti indicates that the peak of the upper HICE excursion occurred during the initial late Hirnantian deglaciation and sea-level rise (6, 24) rather than previous interpretations of it occurring during peak glaciation (e.g., ref. 25). This difference in timing has important implications for the origins of the HICE as being related to increased carbon burial or carbonate weathering during glacial lowstand conditions (11, 26).

In oxidizing seawater, uranium derived from the weathering of continental crust is present mainly as U(VI), as a suite of carbonate and calcium aqueous complexes that form soluble carbonate and phosphate phases (27). Marine U sinks include anoxic/euxinic and suboxic sediments, biogenic carbonates, deltaic sediments, and hydrothermally altered seafloor basalts (28, 29). Within anoxic/euxinic sediments, microbial reduction of U(VI) to U(IV) leads to the formation of relatively insoluble hydroxide and phosphate complexes and organo-metallic ligands (30). Fractionation enriches U(IV) with $^{238}$U leaving the residual U(VI) in seawater depleted in $^{238}$U (28, 30, 31).

$\delta^{238}$U is defined as $[(^{238}U/^{235}U)_{sample}/(^{238}U/^{235}U)_{standard} - 1] \times 1{,}000$, where the standard is NBL-112A (also CRM-112A), which has a $^{238}$U/$^{235}$U ratio of 137.832 ± 0.026 (32, 33). The $\delta^{238}$U trends in marine carbonates have been used to constrain the marine redox history of late Proterozoic through mid-Cretaceous oceans highlighting its use as a globally integrated seawater redox proxy (13–18, 34, 35).

## Results

**U-Isotopic Values.** $\delta^{238}$U values range from −0.79‰ to −0.004‰ and $^{234}$U/$^{238}$U values range from 1.0 to 2.2 (average = 1.45; *SI Appendix*, Table S1). The LOWESS (locally weighted scatterplot smoothing) smoothed curve through the $\delta^{238}$U data captures the general trends across the ~2 My study interval. Average middle Hirnantian values are ~ −0.1‰, followed by a rapid negative 0.3‰ shift, then continue with low, but fluctuating values (average = ~−0.45‰) in the late Hirnantian through early Silurian. The two outlying data points with low $\delta^{238}$U values (−0.79‰) are immediately adjacent to the peak glaciation lowstand unconformity; specifically, the two data points come from 15 cm below the unconformity and within lag deposits lying 15 cm above the unconformity. It is not clear why these samples record such low isotopic values, in particular because samples lying only 50 cm above and below the outliers record $\delta^{238}$U values identical to the overall negative values (Fig. 1). The single outlier at the onset of the abrupt negative shift (−0.79‰) records whole rock and carbonate fraction elemental concentrations that are lower by 2–3 orders of magnitude than all other samples; consequently, we do not include these outlying data points in subsequent discussions.

**Elemental, Total Organic Carbon, and wt% Carbonate Analysis.** Elemental concentrations from the carbonate (carb) and whole (WR) fraction, total organic carbon (TOC), and weight percent carbonate (wt% carb) were analyzed on selected samples to evaluate potential influences from local depositional and diagenetic processes (*SI Appendix*, Figs. S1 and S2 and Table S1). TOC values are low and range from 0.12 to 0.58 wt% with an average of 0.23 wt%; wt% carbonate ranges from 66 to 96% with an average of 86%.

**$\delta^{18}O_{apatite}$ Values.** Samples straddling the peak late Hirnantian glacio-eustatic lowstand were analyzed for $\delta^{18}$O to estimate the magnitude of eustatic sea-level changes during the second LOME pulse. We utilize conodont apatite because, unlike previous calcite $\delta^{18}$O-based studies, apatite is less susceptible to diagenesis than calcite. Due to the low conodont yields across the extinction interval and their small size, individual elements were analyzed using secondary ion mass spectrometry (SIMS). Measured $\delta^{18}$O values range from 17.5‰ to 19.3‰ with values increasing upward toward the peak glacial lowstand unconformity, peak values occur 30 cm above the main unconformity, then decrease into the lowest Silurian (Fig. 1 and *SI Appendix*, Table S1). The minimum magnitude of the positive $\delta^{18}$O shift is 0.8‰ and the overlying negative shift is 2.0‰.

## Discussion

**Influences on Carbonate $\delta^{238}$U.** To evaluate whether the bulk carbonate $\delta^{238}$U values represent global seawater redox conditions rather than trends related to local processes, we discuss various lithologic and geochemical criteria used to evaluate the data. Arguing against local anoxic bottom water conditions controlling the observed $\delta^{238}$U trends is that there is no lithologic evidence for anoxic deposition at any time (*SI Appendix*). The negative $\delta^{238}$U shift in the latest Hirnantian occurs in a continuous succession of bioturbated (suboxic) offshore lime mudstones indicating that the abrupt isotopic shift was not environmentally (facies) controlled. In addition, if local bottom waters were anoxic and controlling measured $\delta^{238}$U values, measured values would be higher rather than lower, and could not explain the observed negative shift. Significantly, the ~65 m thick interval of low, but fluctuating, $\delta^{238}$U values (indicating more reducing seawaters) occurs in a range of bioturbated offshore through upper shoreface and patch reef facies. The patch reef facies were deposited within wave-mixed, photic-zone water depths (oxic), which were presumably in equilibrium with atmospheric oxygen levels; as such, the low isotopic values cannot reflect local anoxic seawaters. Last, high sediment TOC concentrations have been proposed to explain reducing bottom waters or porewaters and thus increased U reduction and sequestration. Low TOC concentrations (average = ~0.2%)

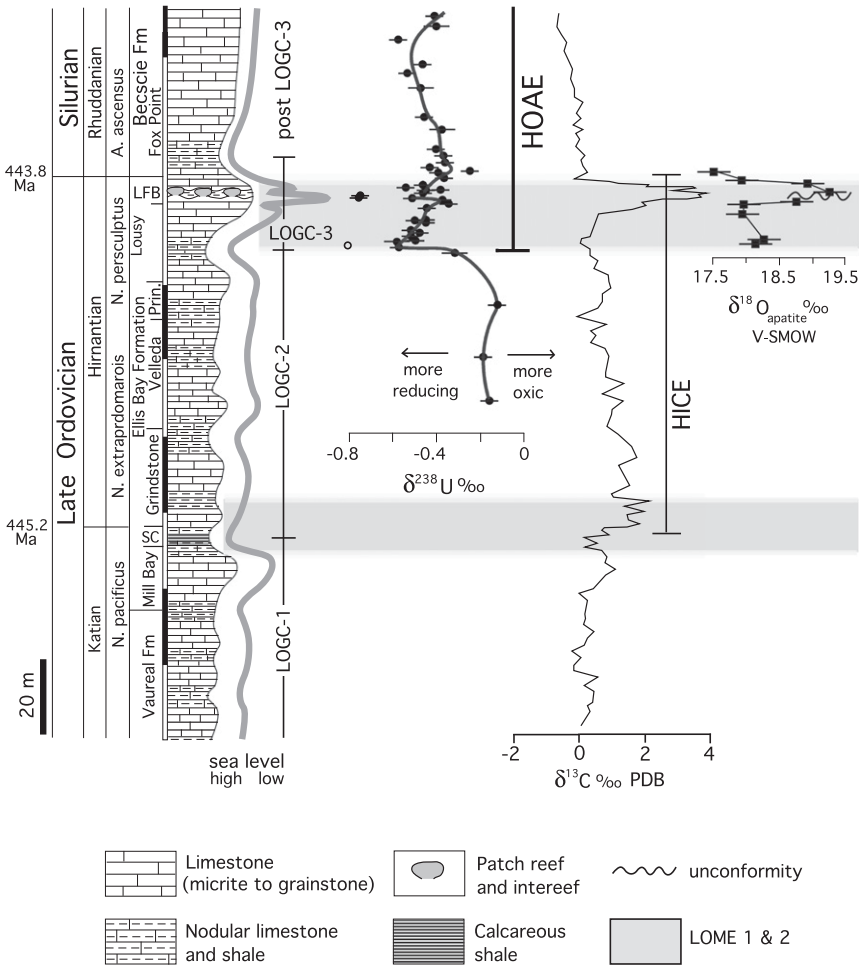


**Fig. 1.** Stratigraphic, glacio-eustatic, $\delta^{238}U$, $\delta^{13}C_{carb}$, and $\delta^{18}O_{apatite}$ records from western Anticosti Island, Canada. The $\delta^{238}U$ curve shown with LOWESS smoothing, which does not include outlying data points with the lowest isotopic values (open circle and two straddling the main unconformity) explained in text. Stratigraphic, sea-level, and $\delta^{13}C_{carb}$ records are from this study, Desrochers et al. (21), and Ghienne et al. (6). HICE, Hirnantian carbon isotope excursion, gray shading represents the two Late Ordovician mass extinction pulses termed LOME 1 (*Lower*) and LOME 2 (*Upper*), HOAE, Hirnantian ocean anoxic event; LOGC, Late Ordovician glacial cycles with boundaries defined by maximum flooding zones from Ghienne et al. (6). Note the main glacial lowstand unconformity at base of LFB (Laframboise member of Ellis Bay Formation). The more minor unconformity at the top of LFB is due to high-frequency eustatic sea-level fall.

throughout the studied succession show no covariance with $\delta^{238}U$ values, suggesting bottom waters were not anoxic (*SI Appendix*, Fig. S2).

To test for the influence of local terrigenous sediment or riverine water input on measured $\delta^{238}U$ values, we compare $\delta^{238}U$ values against wt% carbonate, $Al_{WR}$, $U_{WR}$ (detrital proxies), and $U_{WR}$ against $U_{carb}$ values (*SI Appendix*, Fig. S2); no covariance among these detrital proxies and $\delta^{238}U$ values are observed, nor is there covariance between $U_{WR}$ versus $U_{carb}$, which would indicate influence by detrital U. An additional argument against detrital- or riverwater-derived U controlling the abrupt negative $\delta^{238}U$ shift is that modern river water $\delta^{238}U$ values are higher (average values of $-0.27 \pm 0.16‰$; ref. 31) than typical seawater (20, 28, 29) reflecting the weathering of continental crustal rocks, so any influences by riverine water input should shift marine carbonate values higher rather than lower. This same argument is used to discount the effects of potential meteoric diagenesis during the peak glacio-eustatic lowstand and unconformity development because any secondary meteoric carbonate cement phases precipitated during exposure would shift bulk marine carbonates to higher rather than lower values. Instead, measured $\delta^{238}U$ values directly above and below the glacial lowstand unconformity record some of the lowest values in the section, implying they were not affected by meteoric-water U input. All samples were screened for potential effects of dolomitization (Mg/Ca ratios > 1) and Mn/Sr > 2 for burial diagenesis (all samples passed screening test).

The $^{234}U/^{238}U$ values higher than 1.0 can be interpreted as the result of remobilized $^{234}U$ from Quaternary secondary carbonate cements overprinted on the Ordovician samples or $^{234}U$ added to the carbonate fraction during sample dissolution from the associated insoluble residues (i.e., clays). We argue that $^{234}U$ was added to the carbonate solute fraction during sample dissolution because (*i*) the four pre-HOAE data points have elevated $^{234}U$ values, yet also record enriched $\delta^{238}U$ values; i.e., there is no covariation between $^{234}U/^{238}U$ versus $\delta^{238}U$ (*SI Appendix*, Fig. S2), and (*ii*) the correlation between wt% carbonate vs. $^{234}U/^{238}U$ (*SI Appendix*, Fig. S2).

Any bulk carbonate rock $\delta^{238}U$ value includes the effects of some authigenic U in carbonate cements. If the cements precipitated from oxidizing porewaters, then the cement $\delta^{238}U$ value would be similar to primary seawater precipitates. If the cements precipitated from $O_2$-depleted porewaters that were in partial communication with overlying seawater, then U reduction would

have led to preferential fractionation of $^{238}U$ into the cements, resulting in a positive shift in bulk carbonate $\delta^{238}U$ values relative to the original seawater value (36). However, fractionation would have been near zero in a closed diagenetic system, in which local porewater U was quantitatively taken up by the cements. The studied carbonate samples likely include carbonate cements that shifted bulk carbonate $\delta^{238}U$ values higher relative to the $\delta^{238}U$ of the primary carbonate components (36). This is confirmed by the −0.14‰ offset between the low-Mg rugose coral sample compared with contemporaneous host bulk limestone (*SI Appendix*, Table S1) and results from shallow-buried modern Bahamian carbonate deposits (37) and Neogene drill cores from the Bahama platform (36). We interpret that the entire Late Ordovician–early Silurian $\delta^{238}U$ curve was uniformly shifted to higher isotopic values, but that the observed trends preserve original relative seawater variability. This is interpretation is based on the fact that samples are derived from a relatively homogenous suite of micrite-dominated limestones that experienced similar burial diagenetic conditions and that Anticosti Island O–S deposits were minimally buried (21). Minimal diagenetic alteration is also supported by the preservation of a distinct positive $\delta^{18}O_{carb}$ excursion across the peak Hirnantian cooling and glaciation interval (38). The preservation of primary seawater redox variability by $\delta^{238}U$ values is confirmed by previous studies that report similar $\delta^{238}U$ trends from geographically widespread Upper Permian–Lower Triassic carbonates. In these studies, the various locations experienced different depositional and diagenetic histories, yet they record similar $\delta^{238}U$ values and trends (13, 15, 16).

**Late Ordovician Anoxia.** We focus on the broad isotopic trends (LOWESS smoothed curve in Fig. 1) recorded over the ∼2 My studied interval to understand the overall redox trends rather than attempt to explain individual data points. Interpreting broad redox trends is an approach taken by similar Paleozoic and Mesozoic $\delta^{238}U$ redox studies (13–18). We refer to the measured latest Ordovician–early Silurian negative $\delta^{238}U$ excursion as the Hirnantian ocean anoxic event or HOAE. Its documentation independently confirms previous interpretations of widespread latest Hirnantian–Rhuddanian anoxia based on black shale distribution (11, 26). Using biostratigraphically controlled sedimentation rates for the Hirnantian at Anticosti Island, the HOAE interval represents at least 1 My and the abrupt onset occurred in <20 ky (*SI Appendix*). Future studies on newly recovered core samples from the overlying lower Silurian (middle-late Rhuddanian) carbonates of Anticosti Island will aid in determining the total HOAE duration.

HOAE onset is coincident with the second LOME extinction pulse at Anticosti Island supporting interpretations that anoxia influenced the extinction (Fig. 1). However, the previous extinction hypothesis suggests that widespread anoxic conditions occurred after peak late Hirnantian glaciation and during the subsequent deglacial sea-level rise due to the onset of warming temperatures and rising sea levels to generate anoxia (11, 26). Specifically, the previous hypothesis suggests that deglacial warming lead to increased continental weathering and sediment and nutrient runoff, followed by enhanced primary productivity. The model also calls upon increased meltwater discharge and resultant regional pycnocline strengthening, which combined to expand the oxygen minimum zones (OMZs). The deglacial sea-level rise spread OMZ anoxic waters onto flooded continental shelves ultimately leading to the demise of shelf organisms (3, 11, 26). In contrast, results from this study indicate that the HOAE onset occurred earlier, during eustatic highstand conditions before the peak Hirnantian glaciation, and that anoxic conditions continued during the peak glacial lowstand and ensuing early Silurian deglacial rise. The difference in timing of when anoxia commenced has important implications for LOME extinction–anoxia models, specifically whether anoxia and extinction initiated due to warming (or cooling) climates and glacial highstand (or lowstand) conditions. The timing difference between our study and earlier studies is likely due to previous complications related to temporal mismatches among various stratigraphic sections that were utilized to evaluate glacio-eustasy versus different sections utilized for redox interpretations. Such timing miscorrelations are not encountered in this study because the eustatic sea-level history and $\delta^{238}U$ redox proxy data were derived from the same stratigraphic section, and it is clear that anoxia began before the peak Hirnantian glaciation and continued through the peak lowstand and subsequent early Silurian rise.

The magnitude of $\delta^{18}O_{apatite}$ change across the LOME includes a positive ∼0.8‰ shift coincident with the peak glacio-eustatic fall and a ∼2‰ negative shift during the ensuing eustatic rise and deglacial (Fig. 1). These are minimum magnitudes because erosion along the main lowstand unconformity removed strata at the base of the Laframboise member. If we assume Neogene icehouse oxygen isotopic proportionalities for the effects of ice volume (∼70% of measured isotopic shift) versus seawater temperature (∼30% of measured isotopic shift), then the measured positive 0.8‰ and negative 2‰ shifts equate to glacio-eustatic changes of at least a 50 m sea-level fall and at least a 130 m sea-level rise, respectively. These results are similar to previous estimates of Hirnantian glacio-eustatic magnitudes derived from bulk carbonate $\delta^{18}O$ analysis (50–100 m; refs. 39 and 40) and 70–150 m changes estimated from sequence stratigraphic and erosional unconformity geometries (40, 41). Results from Late Ordovician–early Silurian carbonate-clumped isotope analyses from western Anticosti Island suggest that, in contrast to the Neogene, the majority of the late Hirnantian carbonate $\delta^{18}O$ shift was due to seawater temperature changes with the remaining shift due to the ice-volume effect (42). If this proportionality is correct, then our apatite-based $\delta^{18}O$ shifts would equate to smaller glacio-eustatic magnitude estimates ranging from ∼30 to 65 m, which are significantly lower than previous interpretations, including results from this study.

Given these results, it appears as if there is little, if any, relationship between large glacio-eustatic shifts, associated climate change, and anoxia and raises questions related to previously interpreted anoxia-LOME extinction hypothesis. For example: if anoxic waters spread onto continental shelves during the extinction, why are anoxic facies lacking on Anticosti Island during the HOAE and the LOME, why did the LOME continue during the peak glacial lowstand if anoxic waters presumably receded during the regression, and why are there no biodiversity changes associated the earliest Silurian deglacial rise when deglacial warming, increased nutrient flux, and transgressive conditions presumably occurred? The observation that the HOAE continued during major glacio-eustatic fluctuations indicates that the area of anoxic sediment accumulation (and $^{238}U$ sequestration) was relatively deep (beyond the shelf edge) and was not affected by major flooding and exposure of epeiric seaways. The fact that the HOAE continued for ∼600 ky after the LOME biologic recovery also indicates that sites of anoxic sediment accumulation did not include shallow epeiric seas where the bulk of benthic biota were recovering from the extinction.

The temporal resolution afforded by the Anticosti Island section indicates that the HOAE onset began ∼20 ky before the onset of the upper HICE peak and continued for over ∼600 ky after the HICE. The fact that the HOAE lasted longer than the HICE indicates that the processes influencing global carbon burial rates were temporally, and perhaps spatially, distinct from those influencing global marine anoxia. Temporal decoupling between $\delta^{238}U$ and $\delta^{13}C$ trends is also reported in Cambrian, Devonian, and Permian studies (14–16, 34). This decoupling is not well understood, but has been attributed to changes in OMZ

depths with respect to the shelf edge (16) or due to organic carbon burial in rapidly accumulating deltaic sinks (influencing $\delta^{13}C$ values, but not related to anoxia) rather than from seafloor areas lying below anoxic waters (14).

The minimum duration of the HOAE is similar to previously reported Paleozoic and Mesozoic OAEs, which occurred during greenhouse climates [e.g., Silurian (43); Jurassic and Cretaceous (44)]. Greenhouse OAEs are commonly attributed to reduced seawater oxygen solubility and sluggish ocean circulation related to warm sea surface temperatures (44). In contrast, the HOAE occurred during icehouse and waning icehouse climates and spanned peak glacial conditions when pole-to-equator thermal gradients were presumably steep and thermohaline circulation rates and seawater oxygen solubility were high (45, 46). Such icehouse conditions are typically not thought to be conducive for the development of widespread ocean anoxia.

**HOAE Model.** We interpret that the HOAE was driven by Late Ordovician global cooling and glaciation, which reorganized high-latitude downwelling patterns and rates, and decreased deep-ocean ventilation. In addition, the cooling enhanced upwelling- and eolian-derived nutrient fluxes, which stimulated surface productivity, increased deep-water oxygen consumption, and expanded OMZs. Expanded OMZs resulted in increased areas of anoxic sediment deposition (and $^{238}U$ sequestration) and lead to a negative $\delta^{238}U$ shift in global seawater values. This model is based on recent documentation of lower dissolved $O_2$ concentrations in Pleistocene deep oceans during the last two glacial stages (47–51). These studies interpret that the decrease in deep-water oxygen concentrations was the result of reorganization of high-latitude surface water downwelling patterns and decreased bottomwater advection (ventilation) rates combined with a strengthened efficiency of the global biologic pump and enhanced the flux of organic matter and respired carbon to the deep oceans and further depleted dissolved $O_2$ concentrations. Glacial stage increases in tradewind- and upwelling-derived nutrients may also have contributed to Pleistocene deep-water oxygen declines by increasing surface-water productivity and the resultant consumption of available oxygen (48). These combined processes clearly counteracted the affects of a decrease in dissolved oxygen content related to temperature-related oxygen solubility.

Our interpretation that anoxia continued across the late Hirnantian peak glacial and the subsequent early Silurian deglacial interval is supported by recent interpretations of continued deep-water anoxia throughout the Hirnantian along the western North America margin based on Fe speciation (52). Persistent anoxia suggests that the threshold of intensified ocean circulation and upwelling was reached and maintained throughout this time interval despite major sea-level changes.

**U Cycle Modeling.** A steady-state U cycle model (*SI Appendix*) was utilized to better quantify the effects of the observed $\delta^{238}U$ trends. Modeling results suggest that the total area of anoxic seafloor at the HOAE onset rose to ∼15% from a background value of near zero, and that ∼80% of seawater U was sequestered into anoxic sediment sinks (*SI Appendix*, Fig. S3). For comparison, previous estimates from steady-state U modeling studies across the Late Permian and Late Devonian extinction events interpret increases in the total area of anoxic seafloor of 20% and 15%, respectively, which suggests that the extent of anoxic seafloor during the second LOME pulse was similar in scope to younger "big five" mass extinctions.

## Conclusions

An abrupt Hirnantian–early Rhuddanian ocean anoxic event lasting at least 1 My is detected using $\delta^{238}U$ trends from marine limestones. The lack of anoxic facies in the studied interval combined with the lack of covariance between $\delta^{238}U$ values and redox-sensitive and detrital elemental concentrations, or TOC, supports the interpretation of a global origin for the observed $\delta^{238}U$ trends. Unlike previous Late Ordovician studies, this new global redox record is derived from the same stratigraphic section that documents changes in glacio-eustasy, global carbon budgets, and the Late Ordovician mass extinction, and thus permits direct temporal comparisons among rapid Latest Ordovician–early Silurian paleoenvironmental changes.

The $\delta^{238}U$ trends indicate anoxic conditions were coincident with onset of the second LOME pulse, but lasted longer than the biologic recovery. This independently supports previous interpretations that widespread anoxia was an important aspect of the second LOME pulse, but that it did not apparently affect post-extinction recovery patterns. The HOAE initiated during high sea level before the peak late Hirnantian glaciation and continued through the glacial eustatic lowstand and the ensuing early Silurian deglaciation and sea-level rise indicating that significant climatic change and associated glacio-eustasy had little effect on seawater redox conditions. These patterns also imply that the location of anoxic sediment accumulation occurred in deeper waters beyond the shelf edge. The HOAE occurred during the upper portion of the global Hirnantian positive carbon isotope excursion, but lasted significantly longer suggesting that the controls on $\delta^{13}C$ were partially decoupled from global-ocean redox drivers.

In contrast to most other abrupt Phanerozoic ocean anoxic events, the HOAE occurs during peak icehouse and waning icehouse conditions rather than greenhouse climates. We interpret that the HOAE was driven by global cooling and glaciation, which reorganized thermohaline circulation, decreased deep-ocean ventilation, and enhanced upwelling- and eolian-derived nutrient fluxes stimulating surface productivity, and expanding OMZs. The increase in deep-water seafloor area under anoxic water lead to increased sediment $^{238}U$ sequestration and lower seawater $\delta^{238}U$ values.

Steady-state U cycle modeling results suggest that there was a ∼15% increase in total anoxic seafloor area, and up to 80% of seawater U was sequestered into anoxic sediments during the rapid onset of the HOAE. Such a large percentage of U sequestration implies that the U ocean residence time was significantly shorter in the Late Ordovician than the modern, which would aid in explaining the rapidity (<20 ky) of the observed negative $\delta^{238}U$ shift.

**ACKNOWLEDGMENTS.** We thank Achim Herrmann at Louisiana State University for discussions and elemental sample analysis (funding from ACS PRF 55392-DNI2 to Herrmann), Stephen Romaniello at Arizona State University for analyzing selected samples for U-isotopes and elemental concentrations, and to Eric Albert for picking and preparing conodonts. Partial funding for the study are from an NSF Grant (EAR 17-536) (to M.E.), University of New Mexico Research Allocations Committee, and Geological Society of America Student grants (to R.B.). Secondary ion mass spectrometry work at the University of Edinburgh was funded by a United Kingdom Natural Environment Research Council (NERC) Facility Grant (IMF518/0514) (to J.R.W., M.E., and A.D.).

1. Sheehan PM (2001) The Late Ordovician mass extinction. *Annu Rev Earth Planet Sci* 29:331–364.
2. Harper DAT (2006) The Ordovician biodiversification: Setting an agenda for marine life. *Palaeogeogr Palaeoclimatol Palaeoecol* 232:148–166.
3. Harper DAT, Hammarlund EU, Rasmussen CMØ (2014) End Ordovician extinctions: A coincidence of causes. *Gondwana Res* 25:1294–1307.
4. Brenchley PJ (1994) Bathymetric and isotopic evidence for a short-lived late Ordovician glaciation in a greenhouse period. *Geology* 22:295–298.
5. Finnegan S, Heim NA, Peters SE, Fischer WW (2012) Climate change and the selective signature of the Late Ordovician mass extinction. *Proc Natl Acad Sci USA* 109:6829–6834.
6. Ghienne J-F, et al. (2014) A Cenozoic-style scenario for the end-Ordovician glaciation. *Nat Commun* 5:4485.
7. Zhang T, et al. (2009) Large perturbations of the carbon and sulfur cycle associated with the Late Ordovician mass extinction in South China. *Geology* 37:299–302.
8. Hammarlund EU, et al. (2012) A sulfidic driver for the end-Ordovician mass extinction. *Earth Planet Sci Lett* 331:128–139.

9. Yan D, Chen D, Wang Q, Wang J (2012) Predominance of stratified anoxic Yangtze Sea interrupted by short-term oxygenation during the Ordo-Silurian transition. *Chem Geol* 291:69–78.
10. Jones DS, Fike DA (2013) Dynamic sulfur and carbon cycling through the end-Ordovician extinction revealed by paired sulfate–pyrite δ 34 S. *Earth Planet Sci Lett* 363: 144–155.
11. Melchin MJ, Mitchell CE, Holmden C, Štorch P (2013) Environmental changes in the Late Ordovician-early Silurian: Review and new insights from black shales and nitrogen isotopes. *Geol Soc Am Bull* 125:1635–1669.
12. Brenchley PJ, Marshall JD, Underwood CJ (2001) Do all mass extinctions represent an ecological crisis? Evidence from the Late Ordovician. *Geol J* 36:329–340.
13. Brennecka GA, Herrmann AD, Algeo TJ, Anbar AD (2011) Rapid expansion of oceanic anoxia immediately before the end-Permian mass extinction. *Proc Natl Acad Sci USA* 108:17631–17634.
14. Dahl TW, et al. (2014) Uranium isotopes distinguish two geochemically distinct stages during the later Cambrian SPICE event. *Earth Planet Sci Lett* 401:313–326.
15. Elrick M, et al. (2016) Global-ocean redox variation during the middle-late Permian through Early Triassic based on uranium isotope and Th/U trends of marine carbonates. *Geology* 45:163–166.
16. Lau KV, et al. (2016) Marine anoxia and delayed Earth system recovery after the end-Permian extinction. *Proc Natl Acad Sci USA* 113:2360–2365.
17. Lau KV, Macdonald FA, Maher K, Payne JL (2017) Uranium isotope evidence for temporary ocean oxygenation in the aftermath of the Sturtian Snowball Earth. *Earth Planet Sci Lett* 458:282–292.
18. Jost AB, et al. (2017) Uranium isotope evidence for an expansion of marine anoxia during the end-Triassic extinction. *Geochem Geophys Geosyst* 18:3093–3108.
19. Anderson MB, et al. (2014) A modern framework for the interpretation of $^{238}U/^{235}U$ in studies of ancient ocean redox. *Earth Planet Sci Lett* 400:184–194.
20. Tissot FLH, Dauphas N (2015) Uranium isotopic compositions of the crust and ocean: Age corrections, U budget and global extent of modern anoxia. *Geochim Cosmochim Acta* 167:113–143.
21. Desrochers A, Farley C, Achab A, Asselin E, Riva JF (2010) A far-field record of the end Ordovician glaciation: The Ellis Bay formation, Anticosti Island, eastern Canada. *Palaeogeogr Palaeoclimatol Palaeoecol* 296:248–263.
22. Barnes CR (1988) The proposed Cambrian–Ordovician global boundary stratotype and point (GSSP) in western Newfoundland, Canada. *Geol Mag* 125:381–414.
23. Achab A, Asselin E, Desrochers A, Riva JF (2013) The end-Ordovician chitinozoan zones of Anticosti Island, Québec: Definition and stratigraphic position. *Rev Palaeobot Palynol* 198:92–109.
24. Mauviel A, Desrochers A (2016) A high-resolution, continuous $\delta^{13}C$ record spanning the Ordovician–Silurian boundary on Anticosti Island, eastern Canada. *Can J Earth Sci* 53:795–801.
25. Bergström SM, Saltzman MM, Schmitz B (2006) First record of the Hirnantian (Upper Ordovician) $\delta^{13}C$ excursion in the North American Midcontinent and its regional implications. *Geol Mag* 143:657–678.
26. Page AA, et al. (2007) Were transgressive black shales a negative feedback mechanism modulating glacio-eustatic cycles in the early Palaeozoic icehouse? *Deep-Time Perspectives on Climate Change: Marrying the Signal from Computer Models and Biological Proxies*, The Micropaleontological Society, Special Publications, (The Geological Society, London), pp 123–156.
27. Weyer S, et al. (2008) Natural fractionation of $^{238}U/^{235}U$. *Geochim Cosmochim Acta* 72:345–359.
28. Dunk RM, Mills RA, Jenkins WJ (2002) A reevaluation of the oceanic uranium budget for the Holocene. *Chem Geol* 190:45–67.
29. Stirling CH, Andersen MB, Potter E-K, Halliday AN (2007) Low-temperature isotopic fractionation of uranium. *Earth Planet Sci Lett* 264:208–225.
30. Klinkhammer GP, Palmer MR (1991) Uranium in the oceans: Where it goes and why. *Geochim Cosmochim Acta* 55:1799–1806.
31. Anderson MB, et al. (2016) Closing in on the marine $^{238}U/^{235}U$ budget. *Chem Geol* 420: 11–22.
32. Richter S, et al. (2010) New average values for the n(238 U)/n(235 U) isotope ratios of natural uranium standards. *Int J Mass Spectrom* 295:94–97.
33. Cheng H, et al. (2013) Improvements in $^{230}$ Th dating, $^{230}$ Th and $^{234}$ U half-life values, and U–Th isotopic measurements by multi-collector inductively coupled plasma mass spectrometry. *Earth Planet Sci Lett* 371–372:82–91.
34. Song H, et al. (2017) Uranium and carbon isotopes document global-ocean redox-productivity relationships linked to cooling during the Frasnian-Famennian mass extinction. *Geology* 45:887–890.
35. Montoya-Pino C, et al. (2010) Global enhancement of ocean anoxia during oceanic anoxic event 2: A quantitative approach using U isotopes. *Geology* 38:315–318.
36. Romaniello SJ, Herrmann AD, Anbar AD (2013) Uranium concentrations and $^{238}U/^{235}U$ isotope ratios in modern carbonates from the Bahamas: Assessing a novel paleoredox proxy. *Chem Geol* 362:305–316.
37. Chen X, Romaniello SJ, Herrmann AD, Anbar AD (2016) Diagenetic effects on uranium isotope fractionation in carbonate sediments from the Bahamas. *American Geophysical Union, Fall Conference*, abst. #PP11B-2015.
38. Jones DS, et al. (2011) Terminal Ordovician carbon isotope stratigraphy and glacioeustatic sea-level change across Anticosti Island (Québec, Canada). *Geol Soc Am Bull* 123:1645–1664.
39. Brenchley PJ (1988) Environmental changes close to the Ordovician boundary. *A Global Analysis of the Ordovician–Silurian Boundary*, Bulletin of the British Museum of Natural History (Geology), eds Cocks LRM, Rickards RB, Vol 43, pp 377–385.
40. Brenchley PJ, Marshall JD, Harper DAT, Buttler CJ, Underwood CJ (2006) A late Ordovician (Hirnantian) karstic surface in a submarine channel, recording glacio-eustatic sea-level changes: Meifod, central Wales. *Geol J* 41:1–22.
41. Loi A, et al. (2010) The Late Ordovician glacio-eustatic record from a high-latitude storm-dominated shelf succession: The Bou Ingarf section (Anti-Atlas, southern Morocco). *Palaeogeogr Palaeoclimatol Palaeoecol* 296:332–358.
42. Finnegan S, et al. (2011) The magnitude and duration of Late Ordovician-early Silurian glaciation. *Science* 331:903–906.
43. Cramer BD, Saltzman MR (2005) Sequestration of $^{12}C$ in the deep ocean during the early Wenlock (Silurian) positive carbon isotope excursion. *Palaeogeogr Palaeoclimatol Palaeoecol* 219:333–349.
44. Jenkyns HC (2010) Geochemistry of oceanic anoxic events. *Geochem Geophys Geosyst* 11:Q03004.
45. Vandenbroucke TR, et al. (2010) Epipelagic chitinozoan biotopes map a steep latitudinal temperature gradient for earliest Late Ordovician seas: Implications for a cooling Late Ordovician climate. *Palaeogeogr Palaeoclimatol Palaeoecol* 294:202–219.
46. Elrick M, et al. (2013) Orbital-scale climate change and glacioeustasy during the early Late Ordovician (pre-Hirnantian) determined from $\delta^{18}O$ values in marine apatite. *Geology* 41:775–778.
47. Schmiedl G, Mackensen A (2006) Multispecies stable isotopes of benthic foraminifers reveal past changes of organic matter decomposition and deepwater oxygenation in the Arabian Sea. *Paleocean* 21:PA4213.
48. Jaccard SL, Galbraith ED (2012) Large climate-driven changes of oceanic oxygen concentrations during the last deglaciation. *Nat Geosci* 5:151–156.
49. Hoogakker BA, et al. (2015) Glacial-interglacial changes in bottom-water oxygen content on the Portuguese margin. *Nat Geosci* 8:40–43.
50. Cartapanis O, Bianchi D, Jaccard SL, Galbraith ED (2016) Global pulses of organic carbon burial in deep-sea sediments during glacial maxima. *Nat Commun* 7:10796.
51. Lu Z, et al. (2016) Oxygen depletion recorded in upper waters of the glacial southern Ocean. *Nat Commun* 7:11146.
52. Ahm ASC, Bjerrum CJ, Hammarlund EU (2017) Disentangling the record of diagenesis, local redox conditions, and global seawater chemistry during the latest Ordovician glaciation. *Earth Planet Sci Lett* 459:145–156.